Organic Electronics 13 (2012) 1266–1276

Contents lists available at SciVerse ScienceDirect

Organic Electronics

journal homepage: www.elsevier.com/locate/orgel

Solution processable quinoxaline based molecular materials for organic field effect transistors

Gitish K. Dutta, Satish Patil *

Solid State and Structural Chemistry Unit, Indian Institute of Science, Bangalore 560012, India

ARTICLE INFO

Article history:
Received 24 January 2012
Received in revised form 15 March 2012
Accepted 17 March 2012
Available online 30 March 2012

Keywords:
Quinoxaline
Liquid crystal
D–A–D
Charge transfer
OFET
Mobility

ABSTRACT

Three new solution processable quinoxaline based donor–acceptor–donor (D–A–D) type molecules have been synthesized for application in field effect transistors. These molecules were characterized by UV–visible spectroscopy, thermal gravimetric analysis, differential scanning calorimetry and cyclic voltammetry. DFT calculation gives deeper insight into the electronic structure of these molecules. The crystallinity and morphology features of thin film were investigated using X-ray diffraction. These molecules show liquid crystalline phase confirmed by DSC and optical polarizing microscopy. Investigation of their field effect transistor performance indicated that these molecules exhibited *p*-type mobility up to 9.7×10^{-4} cm^2 V^{-1} s^{-1} and on/off ratio of 10^4.

1. Introduction

Organic field-effect transistors (OFETs) have drawn considerable research interest in recent years because of their potential applications in low-cost, large-area and flexible electronic devices, such as electronic papers [1–3], sensors [4–6], memory devices [7–9] and flexible displays [10,11]. The organic semiconductors have several key advantages over inorganic counterpart such as low-temperature solution processing, readily tunable molecular/polymeric structures, compatibility with flexible organic substrates [12–14] and roll-to-roll manufacture [15]. Developments of new materials which can be easily processable by spin coating, ink-jet printing [16,17] etc. is a very important factor for low cost electronics [18]. Organic small molecules such as pentacene, rubrene are proven to be promising materials for field effect transistors but processing a film requires high cost vacuum deposition technique to fabricate OFET devices [19]. Therefore, in recent years, the solution processable small organic semiconductors for OFET are in great demand [20]. These small molecules have several advantages over polymer semiconductor in terms of crystallinity and purity [21]. Crystallinity of such semiconductors plays important role in determining their charge transport properties [22]. Recently, significant advances have been made in developing stable and possibly solution processable small molecules [23]. Among the small molecules, much of the attention has been focused on the oligoacenes [24,25], thiophene oligomers [26] and perylene derivatives [27]. The reason for this choice is the crystalline nature of these materials, favorable π–π solid state packing and they can be easily processed in solution by functionalization with suitable alkyl chains. Solution processable pentacene derivative 6,13-bis(triiso-propylsilylethynyl)pentacene (TIPS-pentacene) was reported by Anthony and co-workers which shows *p*-type mobility up to 0.4 cm^2 V^{-1} s^{-1} [28]. Similarly, Gundlach and co-workers reported another derivative, 2,8-difluoro-5,11-bis(triethylsilylethynyl)anthradithiophene (diF-TES ADT) with mobility of 0.4 cm^2 V^{-1} s^{-1} for the OFET devices fabricated from spin coated samples [29]. These mobilities number are quite encouraging for plastic electronics with roll to roll manufacture.

* Corresponding author. Tel.: +91 80 22932651; fax: +91 80 23601310.
E-mail address: satish@sscu.iisc.ernet.in (S. Patil).

1566-1199/$ - see front matter © 2012 Elsevier B.V. All rights reserved.
http://dx.doi.org/10.1016/j.orgel.2012.03.012

Another promising approach which has been the subject of recent research work is, organic semiconductors with liquid crystalline properties for the application of organic field-effect transistors [30,31]. The π-conjugated materials with liquid crystalline properties have many advantages arising from spontaneous alignment, narrowly distributed localized states and self-assembling properties [32]. Moreover, Hanna and co-workers have demonstrated that the thin films fabricated by spin coating at liquid crystalline temperature have excellent and uniform morphology and show better FET performance than the devices fabricated with the thin films spin-coated at room temperature in crystalline phase [33].

The carrier transport properties in the discotic columnar phase [34], smectic phase [35,36] and nematic phase [37] have been investigated by time-of-flight (TOF) spectroscopy. High charge carrier mobilities exceeding 0.1 $cm^2 V^{-1} s^{-1}$ have been observed in the highly ordered smectic phases of thiophene derivatives [38].

In this work, we focused on synthesis of π-conjugated materials with donor–acceptor–donor (D–A–D) containing quinoxaline as electron-deficient and electron-rich thiophene backbone. Earlier such quinoxaline based systems had been studied for electroluminescence [39]. The introduction of D–A–D structure in liquid crystalline materials can lower the optical band gap and hence will have potential applications in organic photovoltaics [40]. In addition, presence of both electron rich (donor) and electron deficient (acceptor) unit are expected to show ambipolar charge transport properties in FET [41].

The chromophores containing D–A–D backbone is a promising approach due to enhanced intra-molecular charge transfer (ICT) which results into periodic structures and intermolecular packing in the solid state [42]. In these extended π-conjugated systems the intermolecular charge transfer integral increases which results into decrease of the charge carrier hopping barrier as well as the distribution of energetic and spatial disorder [43].

In this paper, we report the synthesis and characterization of three different quinoxaline based D–A–D derivatives (Scheme 1). In addition, we also discuss the liquid crystalline properties and the influence of the side chain on the carrier transport. The X-ray diffraction studies further gives insight into the solid state packing of these materials.

2. Results and discussions

2.1. Synthesis and characterizations

The synthetic route to target compounds BT-Q, BT-diphQ and BT-dithQ is shown in Scheme 2. The 5,8-dibromo-quinoxalines (a–c) were synthesized according to reported procedure [44] by the condensation reaction of 3,6-dibromobenzene-1, 2-diamine (2) with the corresponding diketocompounds. Tributyl(5′-decyl-[2,2′-bithiophen]-5-yl)stannane (6) was prepared according to method described in literature [45] and the final derivatives (BT-Q, BT-diphQ and BT-dithQ) were synthesized by Stille cross-coupling reaction between 5,8-dibromoquinoxalines and tributyl(5′-decyl-[2,2′-bithiophen]-5-yl)stannane in presence of catalytic amount of $Pd(PPh_3)_4$ and 1:1 toluene and DMF as solvents. All these compounds were purified by column chromatography on silica gel using 1:1 hexane and chloroform as eluent to give red colored solid in good yield and characterized by ^1H, ^{13}C NMR and elemental analysis.

2.2. Electronic absorption and emission spectra

The absorption and photoluminescence spectra of the three new π-conjugated chromophores (BT-Q, BT-diphQ and BT-dithQ) were recorded in chloroform solution. The spectra are illustrated in Fig. 1. There are two distinct absorption peaks observed which belong to $\pi-\pi^*$ transition of the conjugated backbone and intramolecular charge transfer (ICT) transition between bithiophene and quinoxaline unit (see below quantum calculation). Molecule BT-Q shows the $\pi-\pi^*$ transition peaks at 362 nm and the ICT transition at 489 nm. The corresponding emission peak is located at 617 nm. Similarly, BT-diphQ and BT-dithQ show the $\pi-\pi^*$ transition band at 362 nm and 372 nm and the

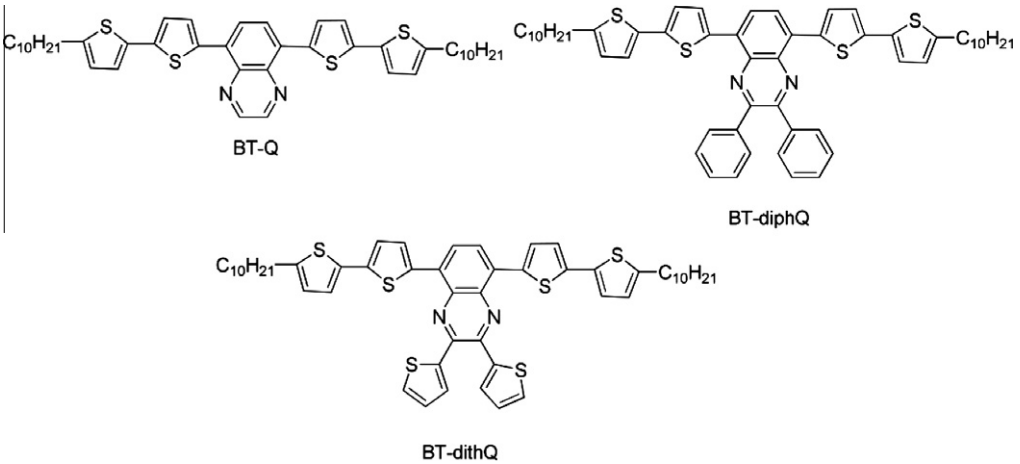

Scheme 1. Chemical structures of the derivatives.

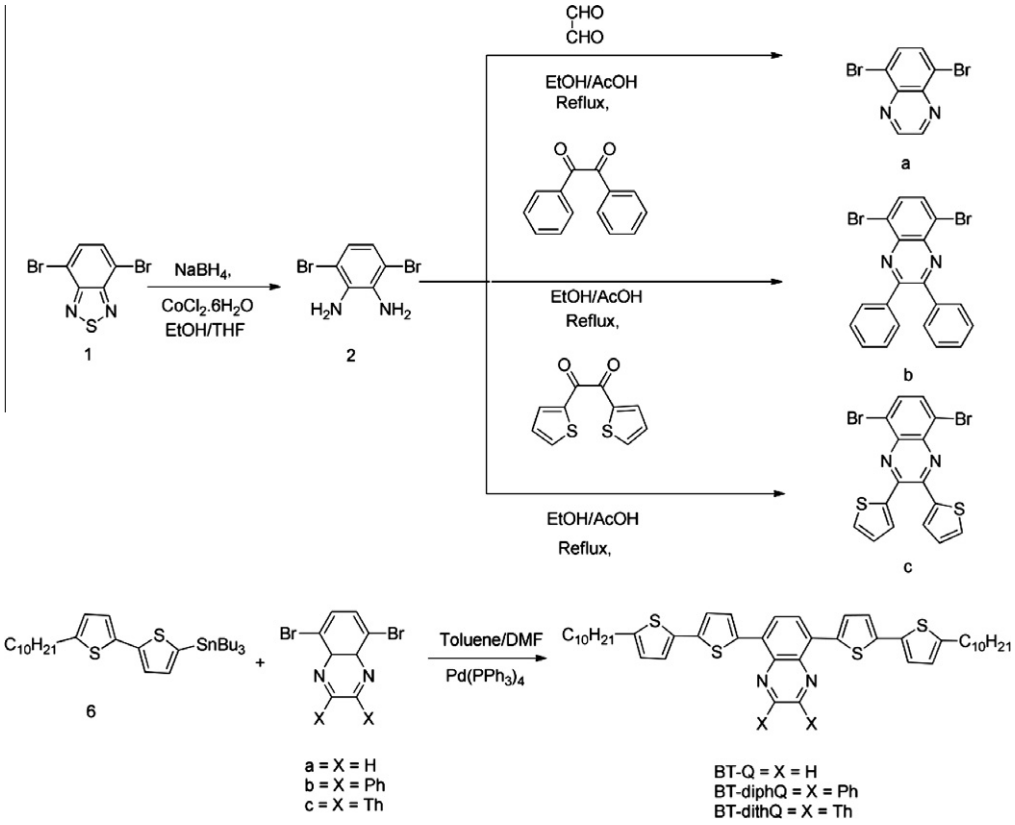

Scheme 2. The synthetic pathway for the compounds BT-Q, BT-diphQ and BT-dithQ.

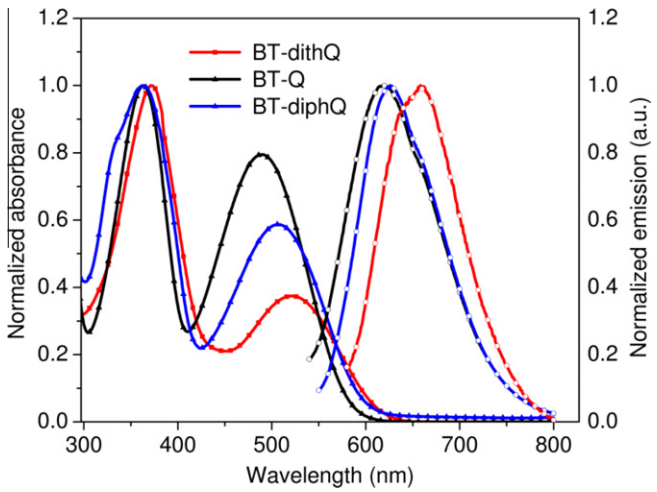

Fig. 1. Absorption and photoluminescence spectra in solution.

ICT transition peak at 506 nm and 521 nm, respectively. The photoluminescence peaks of BT-diphQ and BT-dithQ are positioned at 626 nm and 657 nm. The slight red shifting of absorption maxima from BT-Q to BT-dithQ is because of increase in conjugation of quinoxaline ring with substitution by phenyl and thiophene ring at 2,3 positions and the decrease in intensity of ICT band is due to weakening of ICT transition oscillator strength (Table S1. Supporting information).

Fig. 2 shows the solid state absorption and photoluminescence spectra of BT-Q, BT-diphQ and BT-dithQ. The observed blue shift of absorption maxima in solid state as compared to solution is because of aggregation due to additional intermolecular interactions in solid state [46].

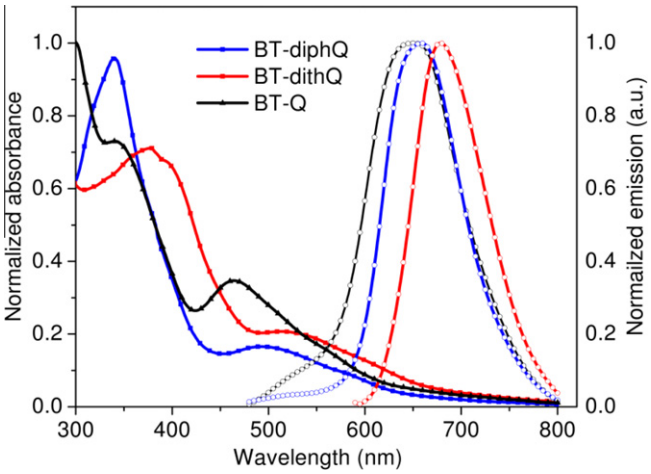

Fig. 2. Absorption and photoluminescence spectra in solid state.

The corresponding emission maxima in the solid state shift to longer wavelengths than those in solution (20–30 nm red shifts) due to strong intermolecular interaction between the molecules (packing effect) [47] in the solid state and more planar geometry in the excited state. The existence of such interaction between neighboring molecules in the solid state is favorable for better device performance. The absorption and photoluminescence maxima in solution and solid state were summarized in Table 1.

2.3. Electrochemical properties

The electrochemical properties of BT-Q, BT-diphQ and BT-dithQ were investigated by cyclic voltammetry using $TBAPF_6$ as supporting electrolyte in dry dichloromethane (DCM) with platinum as working electrodes, a platinum wire counter electrode, and an $Ag/AgNO_3$ reference electrode under Ar atmosphere. All these three molecules show reversible oxidation peak (Fig. 3). The highest occupied molecular orbital (HOMO) were calculated from the oxidation onset of cyclic voltammetry and the LUMO levels were estimated from HOMO values and values of optical band gap according to the Eq. (1) and (2). The optical bandgap (E_g), were approximated from the onset of the low energy side of the absorption spectra (λ_{onset}, solution) to the baseline.

$$\mathrm{HOMO} = -(E_{ox}^{onset} + 4.84)(\mathrm{eV}) \quad (1)$$

$$\mathrm{LUMO} = \mathrm{HOMO} + E_g^{opt}(\mathrm{eV}) \quad (2)$$

The results of the electrochemical measurements and calculated molecular energy levels of these materials are listed in Table 1. It is clear that the HOMO levels are gradually increases with the substitution of the quinoxaline ring with more electron donating phenyl and thiophene rings.

2.4. Theoretical investigation of molecular geometry

The optimized geometry and electronic properties of BT-Q have been investigated by theoretical calculation using Gaussian 03 with hybrid density functional theory (DFT), B3LYP/6–31 g* as basis set. In these calculations, the long alkyl chains were replaced by methyl group in order to reduce computational time.

The electron density of HOMO is distributed all over the conjugated backbone while electron density of LUMO mainly delocalizes on quinoxaline ring and partly on the adjacent thiophene ring indicating intramolecular charge transfer from donor to acceptor unit (Fig. 4) which partly explains the absorption band at 489 nm in UV–visible spectroscopy. The presence of phenyl and thiophene ring in case of BT-diphQ and BT-dithQ increase the torsion angle between thiophene and quinoxaline ring in the backbone (Fig. S1, Supporting information) which further supports the red shift in photoluminescence spectra.

2.5. Thermal properties

The thermal properties of BT-Q, BT-diphQ and BT-dithQ were characterized by thermogravimetric analysis (TGA) and differential scanning calorimetry (DSC). From TGA measurements (at a heating rate of 5 °C under N_2) it has been observed that these derivatives are stable up to 400 °C (Fig. S2, Supporting information). Differential scanning calorimetry (DSC) analyses at a heating rate of 5 °C/min revealed that all three molecules show different types of phase transitions (Fig. 5). BT-Q shows three different endothermic peaks at 166, 183, 236 °C and corresponding exothermic peaks at 86, 179, and 236 °C. The phase existing between temperature ranges of 183 and 236 °C shows smectic A liquid crystalline phase (LC) confirmed from optical polarizing microscopy image studies and the phase present between 166 and 183 °C shows finger print texture under polarizing microscope. On the other hand, BT-diphQ shows only two endothermic peaks at 154 and 183 °C and the corresponding exothermic peaks at 52 and 173 °C. On heating, melting is observed near 154 °C and it forms a glassy state (see Fig. S3, in Supporting information) and near 183 °C it completely transforms to isotropic phase. BT-dithQ shows two endothermic peaks at 118 and 162 °C and one exothermic peak

Table 1
Summary of optical and electrochemical properties.

Compounds	Film		Solution		Bandgap		CV	
	λ_{abs} (nm)	λ_{em} (nm)	λ_{abs} (nm)	λ_{em} (nm)	E_g (eV)	E_{ox}^{onset} (V)	E_{HOMO} [eV]	E_{LUMO} [eV]
BT-Q	463	649	489	617	2.0	0.50	−5.34	−3.34
BT-diphQ	492	658	506	626	2.0	0.46	−5.30	−3.30
BT-dithQ	517	679	521	657	2.0	0.20	−5.04	−3.04

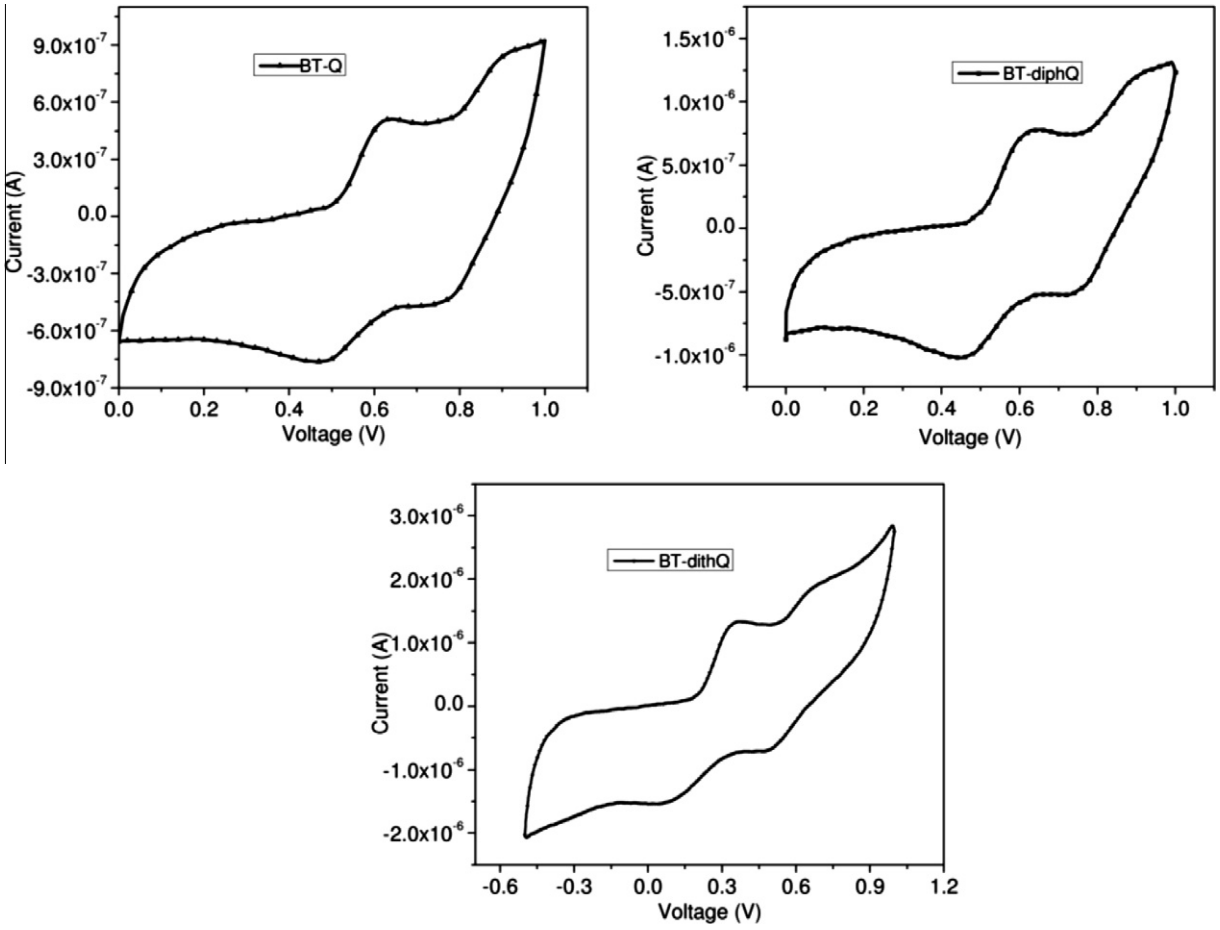

Fig. 3. Cyclic voltametry diagrams.

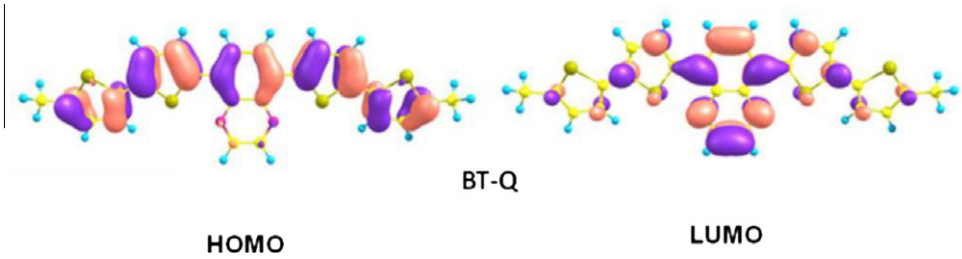

Fig. 4. Molecular orbital surface of HOMO and LUMO of BT-Q.

at 143 °C. On heating, BT-dithQ starts melting near 118 °C and transforms into a glassy state like BT-diphQ (see Fig. S3 in Supporting information) which changes to isotropic phase at 162 °C.

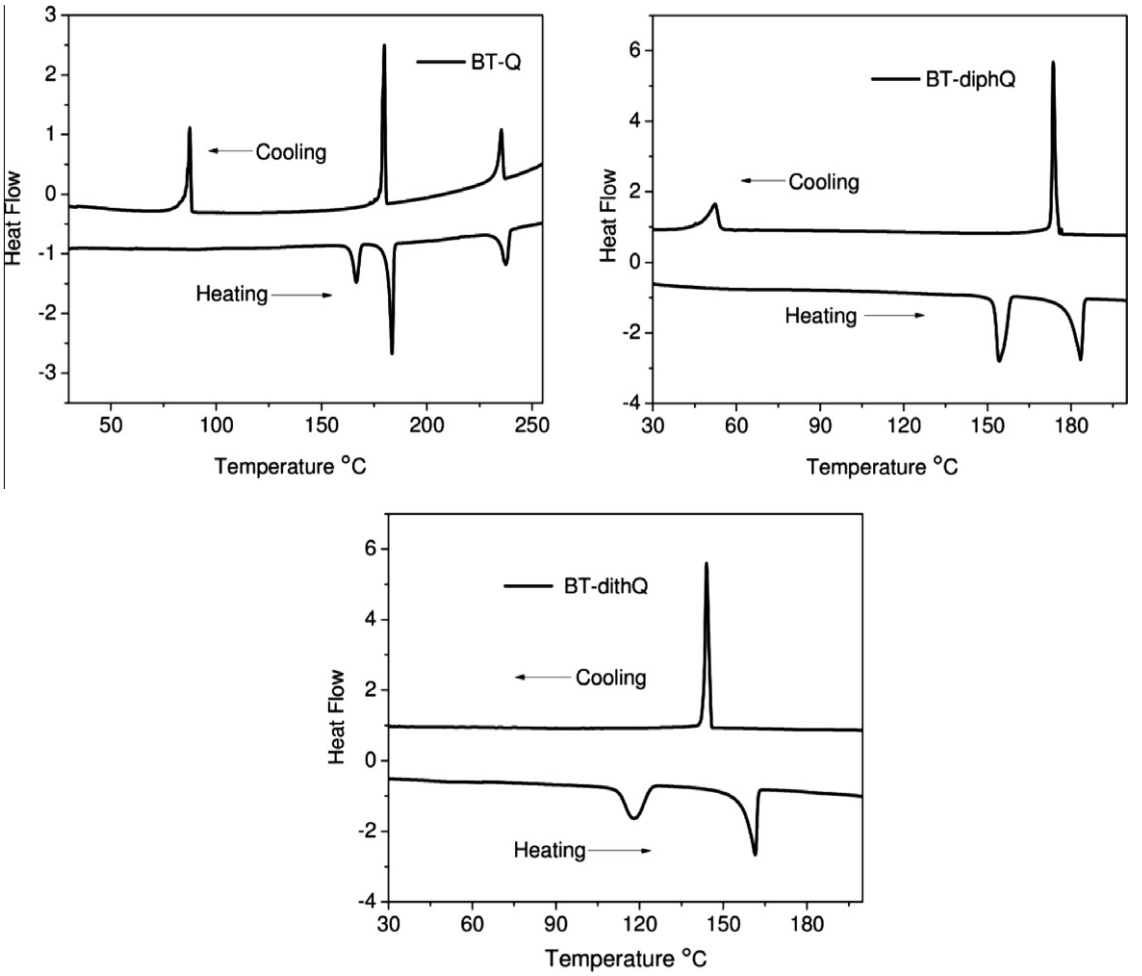

Fig. 5. DSC of BT-Q, BT-diphQ and BT-dithQ.

Molecules BT-diphQ and BT-dithQ did not show any liquid crystalline (LC) phase (under polarizing microscope) due to loss of rigidity of the backbone with substituted by phenyl and thiophene rings. The presence of these phenyl and thiophene ring as a substituent in the backbone does not allow the molecules to pack closely. As a result their melting point also decreases as compared to unsubstituted BT-Q which is evident from DSC.

While cooling BT-Q from isotropic phase, a typical fan-like structure (Fig. 6A) indicating smectic A starts appear-

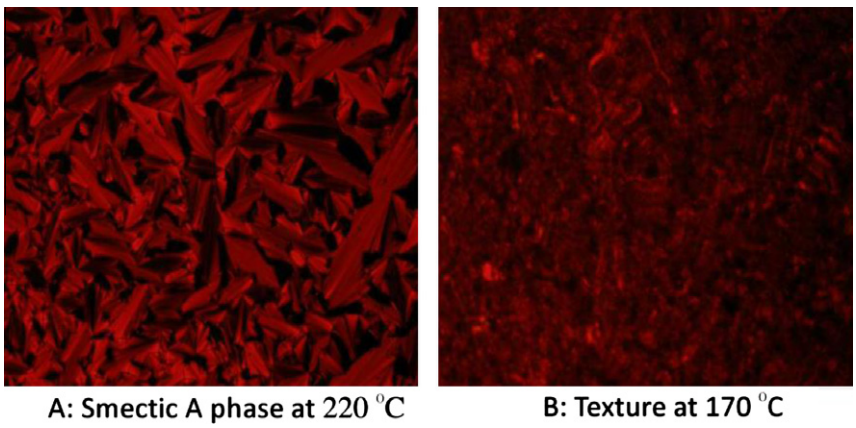

Fig. 6. Optical polarizing image of LC phase of BT-Q.

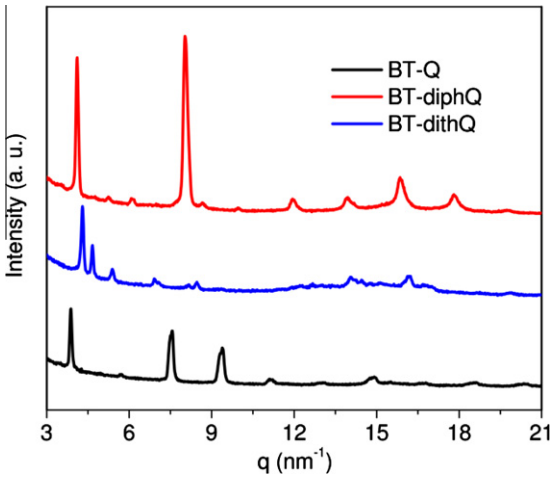

Fig. 7. Thin film XRD of BT-Q, BT-diphQ and BT-dithQ.

ing at around 235 °C and that exists up to 183 °C. Upon further cooling, a fingerprint textures appeared after 183 °C as shown in Fig. 6B which is not conventional molecular crystal, called soft crystal. As mentioned earlier BT-diphQ and BT-dithQ forms a glassy state when it is cooled from isotropic phase and that exists up to room temperature (Fig. S3, Supporting information).

2.6. Thin film XRD

To investigate the crystallinity of the prepared thin film, powder X-ray diffraction (XRD) were performed. Fig. 7 shows the XRD patterns of BT-Q, BT-diphQ and BT-dithQ thin films deposited on octadecyltrichlorosilane (OTS)-treated SiO_2/Si substrates at room temperature by drop casting. The thin films XRD patterns indicate that the materials exhibit good crystallinity behavior with multiple diffraction features suggesting crystalline nature of the

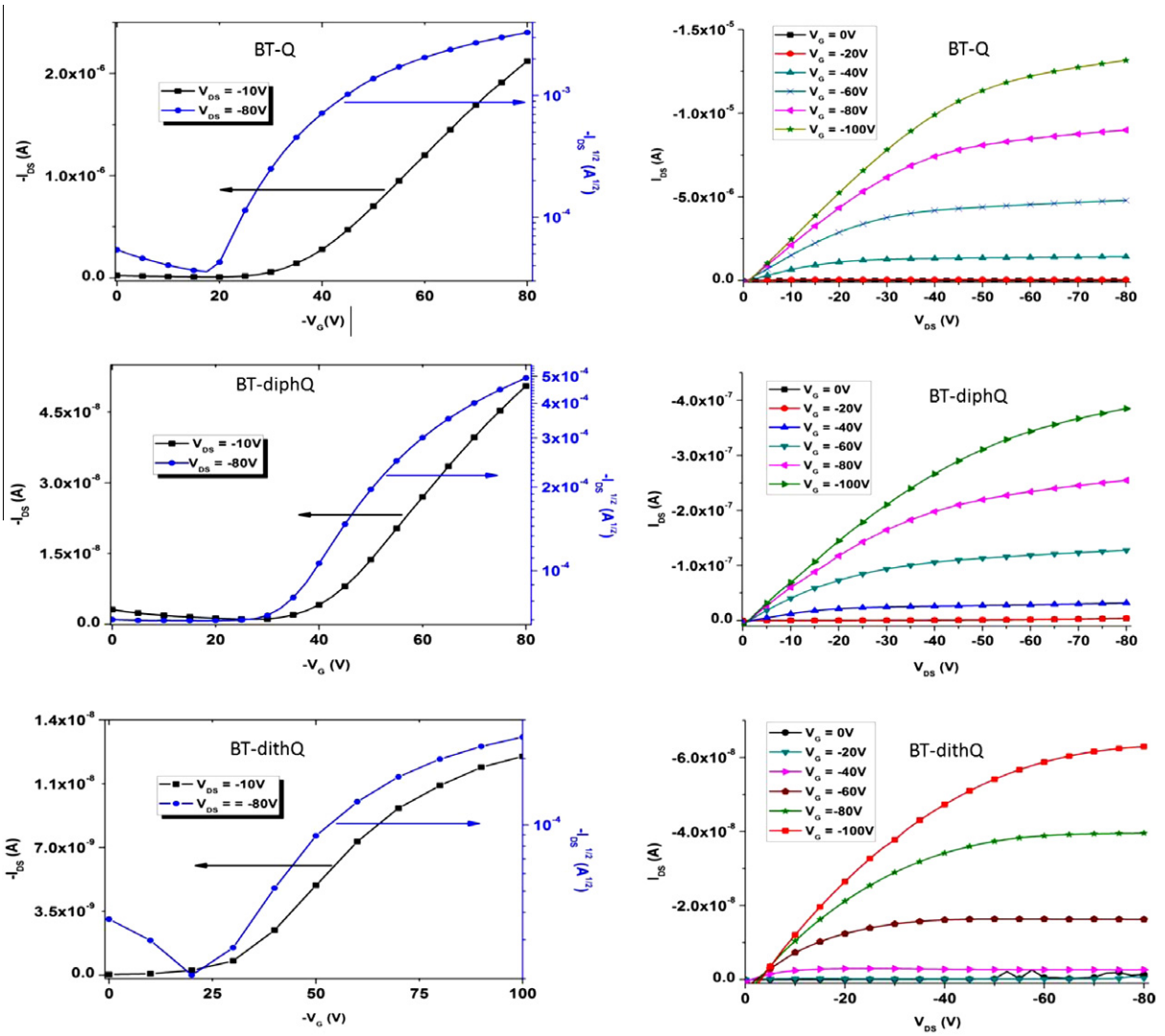

Fig. 8. Transfer and output characteristic curve of BT-Q, BT-diphQ and BT-dithQ.

Table 2
Summary of OFET device characteristics.

Surface	BT-Q	BT-diphQ	BT-dithQ
	HMDS	OTS	HMDS
Mobility (saturated)	9.7×10^{-4} cm^2/V s	6.2×10^{-5} cm^2/V s	6.6×10^{-6} cm^2/V s
On/off ratio	5.2×10^4	84	45
Threshold voltage	−8.1 V	−22.25 V	−19.9 V

samples. Compound BT-Q exhibits distinct diffraction peaks at q (scattering vector) = 3.8, 7.5 and 9.3 nm^{-1} with d-spacings of 16.5 Å, 8.3 Å and 6.7 Å corresponding to different intermolecular distances. Compound BT-diphQ shows two sharp diffraction peaks at q = 4.1 and 8.0 nm^{-1} with d-spacings of 15.3 Å and 7.8 Å. The intermolecular distances calculated for the compound BT-dithQ was found to be 14.6 Å and 11.8 Å from the q values at 4.3 and 5.3 nm^{-1}, respectively. The peak observed at higher q values corresponds to π–π stacking distances. The calculated π–π stacking distances for BT-Q, BT-diphQ and BT-dithQ are found to be 3.38 Å, 3.96 Å and 3.87 Å, respectively. Several other reflections in the higher q values (between 15 and 19 nm^{-1}), occur because of the organization within the 3D lattice [48].

2.7. Characterization of field effect transistor devices

To characterize thin film transistor (TFT) performance, OFET devices for these materials as an active layer were fabricated on n-type SiO_2 substrate. In order to improve the performance of the dielectric layer the surface of SiO_2 was treated with hexamethyldisilazane (HMDS) and octadecyltrimethoxysilane (OTS) as self-assembled monolayer (SAM). The current voltage characteristics of these molecules in OFET are shown in Fig. 8 and summarized in Table 2.

The mobility in the saturated regime was extracted using Eq. (3).

$$I_{DS} = \frac{W}{L}\frac{\mu_{FE}C_{ox}}{2}(V_G - V_t)^2 \quad (3)$$

where I_{DS} is the source-drain current, V_G is the applied gate voltage, V_t is the threshold voltage of the device, W is the channel width, L is the channel length, C_{ox} is the capacitance of the oxide layer and μ_{FE} is the field-effect mobility. The threshold voltage was extracted in the saturated regime by extrapolating to $I_{DS} = 0$. The on/off ratio was calculated at V_{DS} = −100 V and V_G = 0 V and −80 V.

The highest p-type mobility and on/off ratio measured was 9.7×10^{-4} cm^2/V s and 10^4 for the OFET device with BT-Q. The threshold voltage for this device was −8.1 V. The other two derivatives BT-diphQ and BT-dithQ show relatively low mobility of 6.2×10^{-5} and 6.6×10^{-6} cm^2/V s, respectively. The on/off ratio for these two derivatives is very low (Table 2) as compared to compound BT-Q which may be due to very low current. The low mobility values for these solution processed device is because of poor film forming properties of these materials. After annealing the devices, we did not observe any improvement in mobility values. There should not be any charge injection barrier with Au electrode since the HOMO value of BT-Q, BT-dithQ and BT-dithQ (5.34–5.04) is quite close to the electrode work function (5.1 eV).The possible reason for better OFET behavior with BT-Q compared to other two derivatives may be due to its more planar and rigid structure. As mentioned earlier, the presence of phenyl and thiophene rings as side chain in BT-diphQ and BT-bithQ reduces their solid state packing. The presence of liquid crystalline phase in case of BT-Q may probably help better alignment of molecules and increase charge carrier mobilities.

3. Conclusions

In conclusion, we have designed and synthesized three D–A–D type conjugated small molecules consisting of quinoxaline as an acceptor coupled to alkylated bithiophene as donor. These materials can show liquid crystalline phase depending on the flexibility and rigidity of the π conjugated backbone. Optical properties investigations indicated that these new molecules exhibited strong π–π stacking aggregation and long wavelength ICT absorption bands. These results demonstrated that quinoxaline based liquid crystalline materials are good candidates for solution processable electronic devices. To improve the performance of these materials in organic devices, it will be necessary to improve the film morphology. Nevertheless, the chemistry described in this manuscript could be beneficially utilized to further optimize molecular structure and film morphology.

4. Experimental section

All the chemicals were purchased from S.D. Fine Chemicals Ltd., Mumbai, India and Spectrochem Pvt. Ltd., Mumbai, India, except tributyltinchloride and $Pd(PPh_3)_4$ which were purchased from Sigma Aldrich. ^{1}H NMR and ^{13}C NMR spectra were recorded using Bruker 400 MHz. Chemical shifts were given in parts per million and coupling constants (J) in Hertz.

4.1. 5, 8-bis(5′-decyl-[2,2′-bithiophen]-5-yl)quinoxalines

Tributyl(5′-decyl-[2,2′-bithiophen]-5-yl)stannane (3.72 mmol) and 5,8-dibromoquinoxalines (1.65 mmol) were dissolved in 15 mL of dry DMF and 15 mL dry toluene. $Pd(PPh_3)_4$ (50 mg, 0.04 mmol) was added and the mixture was stirred for 24 h at 95 °C under Ar atmosphere. After cooling to room temperature the solvent was removed in rotavapor and extracted the red color solid with $CHCl_3$

and purified by column chromatography (SiO_2/chloroform).

4.2. 5, 8-bis(5′-decyl-[2,2′-bithiophen]-5-yl)quinoxaline (BT-Q)

Yield: 0.98 g (80%).

^{1}H NMR (400 MHz, $CDCl_3$): δ 8.98 (*s*, 2H), 8.11 (*s*, 2H), 7.74–7.73 (*d*,*J* = 4 Hz, 2H), 7.17 (*d*,*J* = 4 Hz, 2H), 7.12–7.11 (*d*,*J* = 4 Hz, 2H), 6.72–6.71 (*d*,*J* = 4 Hz, 2H), 2.81 (*t*,*J* = 8 Hz, 4H), 1.74–1.67 (*m*, 4H), 1.41–1.22 (*m*, 28H), 0.88 (*t*,*J* = 8 Hz, 6H).

^{13}C NMR (100 MHz, $CDCl_3$): δ 145.71, 143.27, 141.12, 139.66, 136.56, 135.01, 131.60, 127.51, 126.93, 124.88, 123.43, 122.80, 31.90, 31.61, 30.24, 29.56, 29.37, 29.32, 29.11, 22.68, 14.10.

Anal, Calcd. for $C_{44}H_{54}N_2S_4$: C, 71.49; H, 7.36; N, 3.79; S, 17.35 found C, 71.35; H, 6.99; N, 5.39; S, 15.06.

4.3. 5,8-bis(5′-decyl-[2,2′-bithiophen]-5-yl)-2,3-diphenylquinoxaline (BT-diphQ)

Yield: 0.74 g (73%).

^{1}H NMR (400 MHz, $CDCl_3$): δ 8.09 (*s*, 2H), 7.79–7.76 (*m*, 6H), 7.40 (*m*, 6H), 7.16–7.15 (*d*,*J* = 4 Hz, 2H), 7.07–7.06 (*d*,*J* = 4 Hz, 2H), 6.72 (*d*,*J* = 4 Hz, 2H), 2.82 (*t*,*J* = 8 Hz 4H), 1.74–1.67 (*m*, 4H), 1.40–1.27 (*m*, 28H), 0.88 (*t*,*J* = 8 Hz, 6H).

^{13}C NMR (100 MHz, $CDCl_3$): δ 151.52, 145.54, 141.05, 138.59, 137.02, 136.80, 135.31, 130.75, 130.60, 129.06, 128.19, 126.96, 126.19, 124.88, 123.14, 122.61, 31.91, 31.62, 30.24, 29.62, 29.58, 29.40, 29.33, 29.13, 22.68, 14.10.

Anal, Calcd. for $C_{56}H_{62}N_2S_4$: C, 75.46; H, 7.01; N, 3.14; S, 14.39 found C, 75.17; H, 6.85; N, 4.94; S, 14.28.

4.4. 5,8-bis(5′-decyl-[2,2′-bithiophen]-5-yl)-2,3-di(thiophen-2-yl)quinoxaline (BT-dithQ)

Yield: 0.468 g (67%).

^{1}H NMR (400 MHz, $CDCl_3$): δ 8.02 (s, 2H), 7.78–7.77 (*d*,*J* = 4 Hz, 2H), 7.58–7.57 (*d*,*J* = 4 Hz, 2H), 7.53–7.52 (*d*,*J* = 4 Hz, 2H), 7.18–7.17 (*d*,*J* = 4 Hz, 2H), 7.13–7.12 (*d*,*J* = 4 Hz, 2H) 7.07–7.05 (*t*,*J* = 4 Hz 2H), 6.74–6.73 (*d*,*J* = 4 Hz, 2H), 2.82 (*t*,*J* = 8 Hz, 4H), 1.73–1.67 (*m*, 4H), 1.40–1.22 (*m*, 28H), 0.86 (*t*,*J* = 8 Hz, 6H).

^{13}C NMR (100 MHz, $CDCl_3$): δ 145.46, 144.47, 141.77, 140.84, 136.61, 136.28, 135.26, 130.14, 129.86, 129.61, 127.38, 127.18, 126.41, 124.82, 123.18, 122.67, 31.86, 31.58, 30.20, 29.57, 29.54, 29.35, 29.29, 29.10, 22.64, 14.08.

Anal, Calcd. for $C_{52}H_{58}N_2S_6$: C, 69.13; H, 6.74; N, 3.10; S, 21.30 found C, 67.59; H, 6.10; N, 4.42; S, 19.61.

4.5. Instruments and measurements

The thermal gravimetric analysis (TGA) was conducted on Mettler Toledo TGA/SDTA 851e instrument (5 °C/min under N_2 atmosphere) and the differential scanning calorimetry (DSC) measurements were done under nitrogen atmosphere on Mettler DSC-1 instrument. The electrochemical properties were examined by using cyclic voltammetry (CH instrument). UV–Vis absorption spectra were recorded on Perkin Elmer (Lambda 35) UV–Vis spectrometer and fluorescence emission spectra were recorded by using Jobin Yvon Fluorolog4. The absorption and fluorescence spectra of solution state were taken in chloroform (conc. 1×10^{-5} mol/L) and that of solid state were recorded from thin film fabricated on quartz substrate by spin coating. Optical polarizing microscopic image of liquid crystalline phase were taken by Olympus-BX-51 polarizing microscope. X-ray diffraction (XRD) patterns were recorded on drop casted thin films of the OTS-treated Si/SiO_2 substrates using PANalytical X'PERT system with Cu Kα (1.541 A). Thermal annealing was carried out on thin film samples for XRD at 120 °C.

4.6. OFET fabrication details

Bottom-gate top contact organic field-effect transistors were fabricated and tested in a glove box under nitrogen. Substrates used were Si, with a silicon oxide layer to act as the gate dielectric. A 350 nm layer of silicon oxide (SiO_2) was grown on a heavily n^{++} doped Si substrate (resistivity 0.001–0.005 Ω/cm) using an HiTech oxidation furnace to form the gate dielectric. The unpolished side of the Si substrate was etched using hydrofluoric acid (HF) to remove the SiO_2, followed by sequential deposition of 4 nm of chromium and 50 nm of gold deposited using thermal evaporation to form the gate electrode. The SiO_2 was cleaned in a Class 1000 clean room by ultarasonication in acetone for 20 min, followed by sonication in 2-propanol for 20 min. Then the substrates were dried in nitrogen. The SiO_2 surface was modified using hexamethyldisilazane (HMDS). An aliquot of 40 μL was pipetted onto the surface and left to stand for 1 min. Substrates were then spun on a spin-coater at 800 rpm for 60 s. Substrates were then baked on a hot plate for 20 min at 110°. Films were formed by spin-coating a 3 mg/mL solution of BT-Q in chlorobenzene (>99.9%, anhydrous). The solution was heated to 70 °C prior to spinning and films were spun hot to ensure the material was properly dissolved in solution. Interdigitated gold source and drain electrodes were formed using vacuum evaporation through a shadow mask prepared using deep reactive ion etching [49]. The final thickness of the electrodes was 30 nm, as measured using a quartz crystal monitor during evaporation. For the best device, the mask used had a length of 90 μm and width of 30 mm. OFETs were tested using Agilent B1500A Semiconductor Device Analyzer and an SA-6 Semi-Auto Prober. For BT-diphQ, SiO_2 substrates were prepared and cleaned as above. The remaining device fabrication steps were performed in a nitrogen filled glove box. The surface of the substrates were modified using octadecyltrimethoxysilane (OTS). Substrates were soaked in a 3 mM OTS solution in toluene (99.8%, anhydrous) for 24 h. Excess of OTS was then removed from the substrates by spinning at 800 rpm for 60 s, with a 30 μL aliquot of toluene dropped onto the substrate surface after 30 s of spinning. Films were formed by spincoating of 4 mg/mL solution of BT-diphQ in chlorobenzene (99.9%, anhydrous) at 1500 rpm for 60 s onto the surface modified substrate. Interdigitated gold electrodes were vacuum evaporated as above to a final thickness of 30 nm. For the best device, the mask used had a channel length of 60 μm and channel width of

10 mm. Device testing is as described previously. The procedure was used for device fabrication of compound BT-dithQ as described for BT-diphQ. The concentration of solution used was 3.2 mg/mL. The device had a length of 100 μm and width of 10 mm.

Acknowledgements

We thank Department of Science and Technology (DST) for financial support and G.K. Dutta thanks UGC for Senior Research Fellowship (SRF). We would like to sincerely acknowledge and thank Prof. Ebinazar Namdas and his groups, University of Queensland, Australia for their help and support for electrical characterization measurements.

Appendix A. Supplementary data

Supplementary data associated with this article can be found, in the online version, at doi:10.1016/j.orgel.2012.03.012.

References

[1] F. Eder, H. Klauk, M. Halik, U. Zschieschang, G. Schmid, C. Dehm, Organic electronics on paper, Appl. Phys. Lett. 84 (2004) 2673.
[2] H. Yan, Z. Chen, Y. Zheng, C. Newman, J.R. Quinn, F. Dötz, M. Kastler, A. Facchetti, A high-mobility electron-transporting polymer for printed transistors, Nature 457 (2009) 679–686.
[3] J.A. Rogers, Z. Bao, K. Baldwin, A. Dodabalapur, B. Crone, V. Raju, V. Kuck, H. Katz, K. Amundson, J. Ewing, Paper-like electronic displays: large-area rubber-stamped plastic sheets of electronics and microencapsulated electrophoretic inks, Proc. Natl. Acad. Sci. USA 98 (2001) 4835.
[4] D.T. McQuade, A.E. Pullen, T.M. Swager, Conjugated polymer-based chemical sensors, Chem. Rev. 100 (2000) 2537–2574.
[5] H. Dong, X. Cao, C.M. Li, Functionalized polypyrrole film: synthesis, characterization, and potential applications in chemical and biological sensors, ACS Appl. Mater. Interfaces 1 (2009) 1599–1606.
[6] H.N. Kim, Z. Guo, W. Zhu, J. Yoon, H. Tian, Recent progress on polymer-based fluorescent and colorimetric chemosensors, Chem. Soc. Rev. 40 (2011) 79–93.
[7] X. Xu, L. Li, B. Liu, Y. Zou, Organic semiconductor memory devices based on a low-band gap polyfluorene derivative with isoindigo as electron-trapping moieties, Appl. Phys. Lett. 98 (2011) 063303.
[8] F. Verbakel, S.C.J. Meskers, R.A.J. Janssen, H.L. Gomes, M. Cölle, M. Büchel, D.M. de Leeuw, Reproducible resistive switching in nonvolatile organic memories, Appl. Phys. Lett. 91 (2007) 192103.
[9] G. de Ruiter, Y.H. Wijsboom, N. Oded, M.E. van der Boom, Polymeric Memory Elements and Logic Circuits that Store Multiple Bit States, ACS Appl. Mater. Interfaces 2 (2010) 3578–3585.
[10] S. Ju, A. Facchetti, Y. Xuan, J. Liu, F. Ishikawa, P. Ye, C. Zhou, T.J. Marks, D.B. Janes, Fabrication of fully transparent nanowire transistors for transparent and flexible electronics, Nat. Nanotechnol. 2 (2007) 378–384.
[11] Z. Bao, J.A. Rogers, H.E. Katz, Printable organic and polymeric semiconducting materials and devices, J. Mater. Chem. 9 (1999) 1895–1904.
[12] A.L. Briseno, R.J. Tseng, M.M. Ling, E.H.L. Falcao, Y. Yang, F. Wudl, Z. Bao, High-performance organic single-crystal transistors on flexible substrates, Adv. Mater. 18 (2006) 2320–2324.
[13] A.L. Briseno, S.C.B. Mannsfeld, M.M. Ling, S. Liu, R.J. Tseng, C. Reese, M.E. Roberts, Y. Yang, F. Wudl, Z. Bao, Patterning organic single-crystal transistor arrays, Nature 444 (2006) 913–917.
[14] G. Gelinck, P. Heremans, K. Nomoto, T.D. Anthopoulos, Organic transistors in optical displays and microelectronic applications, Adv. Mater. 22 (2010) 3778–3798.
[15] F.C. Krebs, J. Fyenbo, M. Jørgensen, Product integration of compact roll-to-roll processed polymer solar cell modules: methods and manufacture using flexographic printing, slot-die coating and rotary screen printing, J. Mater. Chem. 20 (2010) 8994–9001.
[16] M.M. Ling, Z. Bao, Thin film deposition, patterning, and printing in organic thin film transistors, Chem. Mater. 16 (2004) 4824–4840.
[17] H. Sirringhaus, T. Kawase, R. Friend, T. Shimoda, M. Inbasekaran, W. Wu, E. Woo, High-resolution inkjet printing of all-polymer transistor circuits, Science 290 (2000) 2123.
[18] K. Cheng, M.-H. Yang, W.W.W. Chiu, C.-Y. Huang, J. Chang, T.-F. Ying, Y. Yang, Ink-jet printing, self-assembled polyelectrolytes, and electroless plating: low cost fabrication of circuits on a flexible substrate at room temperature, Macromol. Rapid Commun. 26 (2005) 247–264.
[19] S.W. Park, S. Jeong, J.M. Choi, J.M. Hwang, J.H. Kim, S. Im, Rubrene polycrystalline transistor channel achieved through in situ vacuum annealing, Appl. Phys. Lett. 91 (2007) 033506.
[20] S. Allard, M. Forster, B. Souharce, H. Thiem, U. Scherf, Organic semiconductors for solution-processable field-effect transistors (OFETs), Angew. Chem. Int. Ed. 47 (2008) 4070–4098.
[21] M.T. Lloyd, J.E. Anthony, G.G. Malliaras, Photovoltaics from soluble small molecules, Mater. Today 10 (2007) 34–41.
[22] V. Coropceanu, J. Cornil, D.A. da Silva Filho, Y. Olivier, R. Silbey, J.-L. Brédas, Charge transport in organic semiconductors, Chem. Rev. 107 (2007) 926–952.
[23] A.C. Arias, J.D. MacKenzie, I. McCulloch, J. Rivnay, A. Salleo, Materials and applications for large area electronics: solution-based approaches, Chem. Rev. 110 (2010) 3–24.
[24] J.E. Anthony, Functionalized acenes and heteroacenes for organic electronics, Chem. Rev. 106 (2006) 5028–5048.
[25] M.M. Payne, S.R. Parkin, J.E. Anthony, C.-C. Kuo, T.N. Jackson, Organic field-effect transistors from solution-deposited functionalized acenes with mobilities as high as 1 cm^2/V s, J. Am. Chem. Soc. 127 (2005) 4986–4987.
[26] M. Mushrush, A. Facchetti, M. Lefenfeld, H.E. Katz, T.J. Marks, Easily processable phenylene–thiophene-based organic field-effect transistors and solution-fabricated nonvolatile transistor memory elements, J. Am. Chem. Soc. 125 (2003) 9414–9423.
[27] C. Piliego, D. Jarzab, G. Gigli, Z. Chen, A. Facchetti, M.A. Loi, High electron mobility and ambient stability in solution-processed perylene-based organic field-effect transistors, Adv. Mater. 21 (2009) 1573–1576.
[28] C.D. Sheraw, T.N. Jackson, D.L. Eaton, J.E. Anthony, Functionalized pentacene active layer organic thin-film transistors, Adv. Mater. 15 (2003) 2009–2011.
[29] O.D. Jurchescu, S. Subramanian, R.J. Kline, S.D. Hudson, J.E. Anthony, T.N. Jackson, D.J. Gundlach, Organic single-crystal field-effect transistors of a soluble anthradithiophene, Chem. Mater. 20 (2008) 6733–6737.
[30] I. McCulloch, M. Heeney, C. Bailey, K. Genevicius, I. MacDonald, M. Shkunov, D. Sparrowe, S. Tierney, R. Wagner, W. Zhang, Liquid-crystalline semiconducting polymers with high charge-carrier mobility, Nat. Mater. 5 (2006) 328.
[31] H. Sirringhaus, R. Wilson, R. Friend, M. Inbasekaran, W. Wu, E. Woo, M. Grell, D. Bradley, Mobility enhancement in conjugated polymer field-effect transistors through chain alignment in a liquid-crystalline phase, Appl. Phys. Lett. 77 (2000) 406.
[32] T. Yasuda, H. Ooi, J. Morita, Y. Akama, K. Minoura, M. Funahashi, T. Shimomura, T. Kato, π-Conjugated Oligothiophene-based polycatenar liquid crystals: self-organization and photoconductive, luminescent, and redox properties, Adv. Funct. Mater. 19 (2009) 411–419.
[33] H. Iino, J.-I. Hanna, Availability of liquid crystallinity in solution processing for polycrystalline thin Films, Adv. Mater. 23 (2011) 1748–1751.
[34] H. Iino, J. Hanna, R.J. Bushby, B. Movaghar, B.J. Whitaker, M.J. Cook, Very high time-of-flight mobility in the columnar phases of a discotic liquid crystal, Appl. Phys. Lett. 87 (2005) 132102.
[35] M. Funahashi, J.-i. Hanna, Fast hole transport in a new calamitic liquid crystal of 2-(4′-heptyloxyphenyl)-6-dodecylthiobenzothiazole, Phys. Rev. Lett. 78 (1997) 2184.
[36] M. Funahashi, F. Zhang, N. Tamaoki, High ambipolar mobility in a highly ordered smectic phase of a dialkylphenylterthiophene derivative that can be applied to solution-processed organic field-effect transistors, Adv. Mater. 19 (2007) 353–358.
[37] K.L. Woon, M.P. Aldred, P. Vlachos, G.H. Mehl, T. Stirner, S.M. Kelly, M. O'Neill, Electronic charge transport in extended nematic liquid crystals, Chem. Mater. 18 (2006) 2311–2317.
[38] M. Funahashi, J.I. Hanna, High carrier mobility up to 0.1 $cm^2 V^{-1} s^{-1}$ at ambient temperatures in thiophene-based smectic liquid crystals, Adv. Mater. 17 (2005) 594–598.

[39] X. Zhang, A.S. Shetty, S.A. Jenekhe, Electroluminescence and photophysical properties of polyquinolines, Macromolecules 32 (1999) 7422–7429.
[40] K. Yao, L. Chen, Y. Chen, F. Li, X. Ren, H. Wang, Y. Li, Tuning the photovoltaic parameters of thiophene-linked donor-acceptor liquid crystalline copolymers for organic photovoltaics, Polym. Chem. 3 (2012).
[41] T.T. Steckler, X. Zhang, J. Hwang, R. Honeyager, S. Ohira, X.-H. Zhang, A. Grant, S. Ellinger, S.A. Odom, D. Sweat, D.B. Tanner, A.G. Rinzler, S. Barlow, J.-L. Brédas, B. Kippelen, S.R. Marder, J.R. Reynolds, A spray-processable, low bandgap, and ambipolar donor−acceptor conjugated polymer, J. Am. Chem. Soc. 131 (2009) 2824–2826.
[42] T. Yasuda, T. Imase, Y. Nakamura, T. Yamamoto, New alternative donor−acceptor arranged poly(aryleneethynylene)s and their related compounds composed of five-membered electron-accepting 1,3,4-thiadiazole, 1,2,4-triazole, or 3,4-dinitrothiophene units: synthesis, packing structure, and optical properties, Macromolecules 38 (2005) 4687–4697.
[43] J.-L. Brédas, D. Beljonne, V. Coropceanu, J. Cornil, Charge-transfer and energy-transfer processes in π-conjugated oligomers and polymers: a molecular picture, Chem. Rev. 104 (2004) 4971–5004.
[44] M.J. Edelmann, J.-M. Raimundo, N.F. Utesch, F. Diederich, C. Boudon, J.-P. Gisselbrecht, M. Gross, Dramatically enhanced fluorescence of heteroaromatic chromophores upon insertion as spacers into oligo(triacetylene)s, Helv. Chim. Acta. 85 (2002) 2195–2213.
[45] C. Zhao, Y. Zhang, M.-K. Ng, Derivatives of 4,9-dihydro-s-indaceno[1,2-b:5,6-b′]dithiophene-4,9-dione: synthesis and properties, J. Org. Chem. 72 (2007) 6364–6371.
[46] X. Zhang, J.P. Johnson, J.W. Kampf, A.J. Matzger, Ring fusion effects on the solid-state properties of – oligothiophenes, Chem. Mat. 18 (2006) 3470–3476.
[47] S. Tirapattur, M. Belletête, N. Drolet, M. Leclerc, G. Durocher, Steady-state and time-resolved studies of 2,7-carbazole-based conjugated polymers in solution and as thin films: determination of their solid state fluorescence quantum efficiencies, Chem. Phys. Lett. 370 (2003) 799–804.
[48] K. Oikawa, H. Monobe, K. Nakayama, T. Kimoto, K. Tsuchiya, B. Heinrich, D. Guillon, Y. Shimizu, M. Yokoyama, High carrier mobility of organic field-effect transistors with a thiophene–naphthalene mesomorphic semiconductor, Adv. Mater. 19 (2007) 1864–1868.
[49] M. Aljada, K. Mutkins, G. Vamvounis, P. Burn, P. Meredith, High quality shadow masks for top contact organic field effect transistors using deep reactive ion etching, J. Micromech. Microeng. 20 (2010) 075037.